LIMNOLOGY
and
OCEANOGRAPHY: METHODS

ASLO

Limnol. Oceanogr.: Methods 2025

doi: 10.1002/lom3.10692

NEW METHODS

A novel, self-contained benthic chamber design for conducting freshwater ecosystem experiments

Jonathan W. Lopez ,* **Matthew B. Lodato, Taylor C. Michael, Lauren M. Morris, Carla L. Atkinson**
Department of Biological Sciences, The University of Alabama, Tuscaloosa, Alabama, USA

Abstract

We present a newly developed design for a self-contained benthic chamber for conducting in situ ecosystem experiments in streams, with a focus on biogeochemical processes such as ecosystem metabolism and nutrient cycling. Our design expands upon smaller, portable chamber designs and is meant to answer questions at larger scales. These new chambers allow for a high level of experimental control in the field and can be used to generate spatially explicit data regarding ecosystem processes and to test mechanistic hypotheses. They are built to be deployed within the stream over periods of weeks to months and to withstand natural hydraulic forces of the benthic zone. First, we describe the materials and steps that are needed to construct these chambers in detail. Then, we report the methods and results of a multi-part, diagnostic field study meant to demonstrate the performance and utility of the design. We quantified solute dynamics using a conservative tracer injection, then we estimated ecosystem metabolism across the study site and performed nutrient additions. We detected asymptotic declines in tracer concentrations, calculated nutrient removal rates, and mapped hotspots of ecosystem metabolism. Flow velocity and water depth imposed limitations, but with appropriate methodological forethought these limitations can be minimized. The capacity of our design to accommodate complex, three-dimensional habitats and macrofauna, along with the capability to generate spatially explicit data, are the main advances we present. These advances provide a novel method whereby motivated users can connect mechanistic hypothesis testing with natural ecological processes through ecosystem-level field experiments.

Stream ecosystems form a vital network for the global transport, storage, and transformation of energy and matter in the forms of carbon and nutrients (Cole et al. 2007; Battin et al. 2009; Hotchkiss et al. 2015; Maranger et al. 2018). Much of the biogeochemical activity that governs the pools and fluxes of carbon and nutrients in streams takes place in the benthic zone (Tank et al. 2000; Hall et al. 2009; Dodds et al. 2013). Therefore, stream ecologists have long sought to generate a mechanistic understanding of the factors driving benthic primary production, ecosystem respiration (ER), and nutrient dynamics in streams, and to extrapolate their estimates of these fundamental ecosystem functions to larger scales (Minshall 1988; Hall et al. 2013). One of the most popular methods to precisely quantify stream ecosystem function and experimentally test which mechanisms drive them is the use of self-contained, isolated benthic chambers (Duff et al. 1984; Bott et al. 1997; Dodds and Brock 1998; Rüegg et al. 2015).

Benthic chambers used by stream ecologists have taken many forms over the years, but all chamber designs come with inherent trade-offs between cost, realism, and experimental control. For example, smaller, simpler chambers with fewer parts may be easier and cheaper to produce but may cause issues with light attenuation and may not allow the manipulation of flow conditions (Dodds and Brock 1998). Among the most widely used contemporary chamber designs is the rectangular, modular design of Rüegg et al. (2015) where a known volume of water circulates in a vertical loop driven by a propeller. Water travels over a sediment sample resting on an internal table, then beneath the table and back around to the other end of the chamber. The design was meant to resolve a

*Correspondence: jwlopez@ua.edu

Associate editor: Mike DeGrandpre
Data Availability Statement: The data used in this manuscript are publicly available at https://doi.org/10.6084/m9.figshare.28430789.v1.

range of issues that were prevalent among earlier chambers, including portability and durability, high chamber volume to sample-area ratios, and flow velocity control. However, this design, like all chambers, has limitations—chiefly their small size and the fact that sediments must still be removed from the benthos and translocated into the chamber during setup.

Marine ecologists, on the other hand, have developed benthic chamber designs which can be lifted on and off the sediment surface directly, allowing ecosystem processes to be measured in situ with minimal disruption to the environment (Kellogg et al. 2013; Humphries et al. 2016; Roth et al. 2019; Gadeken et al. 2023). These chambers are generally larger in volume and cross-sectional area, allowing ecologists to not just assess the impacts of microbes, algae, and meiofauna, but also complex, three-dimensional habitats that include macrofauna such as corals and bivalves (Roth et al. 2019). However, these chambers are typically cylindrical or cubical, and these shapes can create substantial drag under unidirectional flow conditions (Vogel 1996). Combined with their larger size, these hydrodynamic limitations have so far made such a design untenable in stream ecosystems (but *see* Fuller and Bucher 1991). Our goal was to design an analogous chamber for use in stream benthic ecosystems which could accommodate three-dimensional environments and macrofauna in situ.

The self-contained chamber design we describe below overcomes the hydrodynamic limitations imposed by cylindrical or cubical chambers by using a dome-shaped design. Our chambers require the installation of a cylindrical polyvinylchloride (PVC) base directly into the benthic zone. At any time, a domed acrylic lid can be fastened to the base to isolate a cross section of the benthic habitat. Inside the assembled chamber, a recirculating pump maintains a current, while loggers record the desired data. The domes also feature resealable sampling ports, which can be used to take water samples over the course of an incubation. The chamber bases are meant to be deployed for weeks to months, allowing natural ecosystem processes to occur in the sediments. Longer deployments allow the user to sample the same cross section of the benthos repeatedly and quantify temporal variation. Further, the measurements are spatially explicit, and with appropriate experimental design, they can be used to model spatial variation in biogeochemical processes at the stream reach scale.

Here, we detail (1) the specific materials used to construct these chambers and the procedures necessary for effective deployment, (2) a field assessment where we first tested solute dynamics in the chambers using a conservative tracer and then demonstrated their applications in benthic metabolism and nutrient dynamics, (3) the strengths and limitations of the design, especially in comparison to smaller portable benthic chambers, and (4) recommendations for future use.

Materials and procedures

Materials

As outlined earlier, the chambers we constructed had two main parts: the chamber base (Fig. 1a) and the chamber dome (Fig. 1b). Each of these main parts is composed of several pieces, most of which are publicly available for purchase either online or in a local hardware store. We have included a list of all the specific components from Fig. 1, including the origins and costs of the specific parts we used (Table 1). However, it is important to note that analogous parts could be obtained from a variety of sources and that costs are not static among suppliers or times of purchase. We constructed 40 chamber bases and 12 domes for the present study. We estimate the cost of the bases at ~ $400 each, with the most expensive

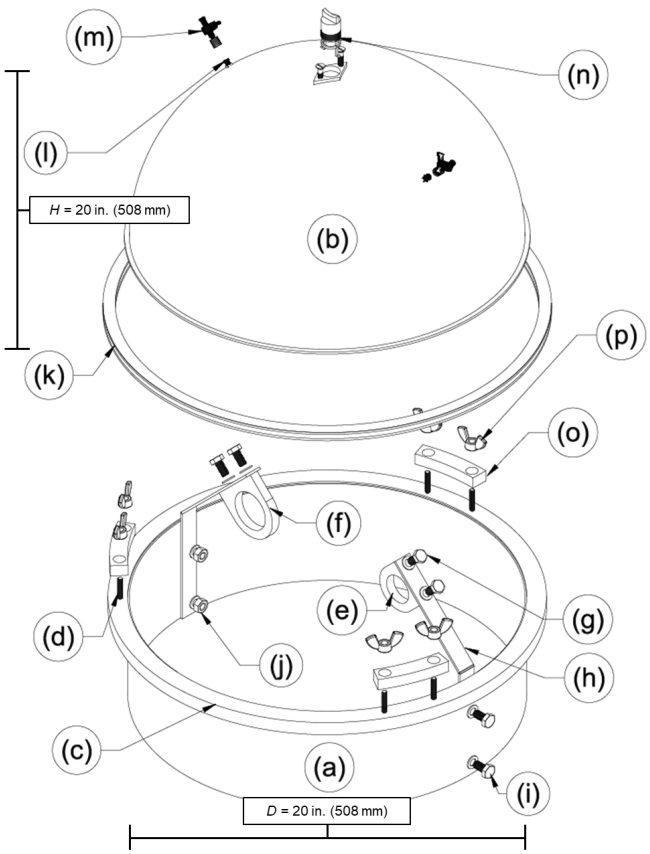

Fig. 1. Schematic of the benthic chamber design described and deployed in this study. The diameter, *D*, of the chamber base and height, *H*, of the chamber dome are shown in text boxes with corresponding scale bars. The field of view is shown at a 45° downward angle, which leads to some distortion of the relative lengths of *H* and *D* in the figure. Details on the annotated parts can be found in Table 1. Briefly, the parts are: (**a**) chamber base, (**b**) chamber dome, (**c**) lip, (**d**) machine screw, (**e**) dissolved oxygen logger holster, (**f**) recirculating pump holster, (**g**) hex cap screw with washer, (**h**) holster arm, (**i**) hex cap screw with washer, (**j**) hex nut with washer, (**k**) rubber lip, (**l**) female luer connection, (**m**) one-way stopcock with male-to-female luer connection, (**n**) drain plug, (**o**) bracket, and (**p**) wingnut.

Table 1. A list of component pieces required to construct the self-contained benthic incubation chambers and their unit costs and origins. Lengths and sizes are given in imperial units in parentheses, and in metric units in brackets. Cost does not include shipping, taxes, or fees. Many items receive a discount when purchased in bulk.

Item	Origin	Label in Fig. 1	Part number	Cost
Chamber base	Commercial Industry Supply	a	1034-CP-20	\$66.00 ft^{-1}
Chamber dome	EZ Tops WorldWide	b		\$97.95 each
Cast acrylic sheet (48-in × 48-in × 0.708-in) [1219 mm × 1219 mm × 18 mm]	US Plastic	c (acrylic lip) o (acrylic bracket)	44,251	\$621.66 each
Machine screw (0.25-in–20 × 2-in) [6-mm × 51 mm]	Everbilt	d	802,862	\$8.98 (pack of 10)
Aluminum bar (12-ft × 3.5-in × 0.5-in) [366-cm × 89 mm × 13 mm]	OnlineMetals.com	e (dissolved oxygen logger holster) f (recirculating pump holster)	17,665	\$156.63 each
Hex cap screw (0.25-in–20 × 0.75-in) [6-mm × 19-in]	McMaster-Carr	g, i	92240A540 92147A029	\$5.90 (pack of 50) \$7.01 (pack of 100)
Washer (split lock 0.25-in) [6-mm]				
Aluminum bar (12-ft × 2.5-in × 0.375-in) [366-cm × 64-mm × 10 mm]	OnlineMetals.com	h (aluminum holster arm)	1158	\$81.15 each
Hex nut (0.25-in–20) [6-mm]	McMaster-Carr	j	95505A601	\$7.08 (pack of 100)
Washer (split lock 0.25-in) [6-mm]			92147A029	\$7.01 (pack of 100)
Rubber trim (style 2, EPDM, 0.25-in × 0.50-in) [6-mm × 13-mm]	McMaster-Carr	k (rubber lip)	8693 K13	\$187.20 (100-ft)
Female luer connection	McMaster-Carr	l	51,525 K439	\$10.71 (pack of 10)
One-way stopcock with male-to-female luer connection	QWORK	m		\$19.97 (pack of 20)
Drain plug	Amazon	n (1-in boat drain plug)		\$6.86 each
	MSC Direct	n (vulcanized fiber washer)		\$32.29 (pack of 25)
Wingnut (style 1, 0.25-in–20) [6-mm]	McMaster-Carr	p	92001A321	\$7.63 (pack of 25)

component being the acrylic lip (~ \$300 per base). The cost of the domes was ~ \$115 each. Costs will vary depending on the desired number of chambers and depending on the specific parts and materials used for construction. For example, we used scrap acrylic that we already had available, which reduced the cost of production from \$400 to closer to \$100 per chamber base. For parts which were purchased or constructed in the United States using imperial measurement units, we provide the relevant measurements in inches (in) or feet (ft) with metric equivalents (to the nearest mm or cm, respectively) presented parenthetically in the narrative.

Chamber base

The primary component of the chamber base is a cylindrical piece of 20-in (501-mm) diameter PVC duct coupling, cut to a height of 6 in (152 mm) (Fig. 1a). At the top of the duct coupling, we attached a circular piece of acrylic of equal diameter using nontoxic waterproof aquarium sealant (Fig. 1c). We cut these acrylic pieces using a water jet in a computerized numerical control mill at the University of Alabama machine shop (CNC Toolroom Mill, Haas Automation). We tapped holes for a series of 0.25-in by 2-in (6-mm by 51-mm) machine screws, which were threaded up through the circular acrylic lip to serve as an attachment point for the chamber domes (Fig. 1d). We inserted the machine screws in three equidistant pairs around the circumference of the acrylic lip and used them as an attachment point for the chamber domes. The final components of the chamber bases were two custom aluminum holsters (Fig. 1e,f). The holsters were also cut at the on-campus machine shop using the computerized numerical control mill. One of the two holsters was cut to match the diameter of a dissolved oxygen logger (Fig. 1e), while the other one was cut to match the diameter of a recirculating water pump (Fig. 1f). We used two 0.25-in by 0.75-in (6-mm by 19-mm) hex cap screws with 0.25-in (6-mm) washers (Fig. 1g) to attach each holster to one of two aluminum arms (Fig. 1h), which extended upward from the base at an angle of ~ 45°. We secured the bottom of each holster arm to the interior of the PVC duct coupling using two additional 0.25-in by 0.75-in (6-mm by 19-mm) hex cap screws and washers (Fig. 1i) and corresponding 0.25-in (6-mm) hex nuts and washers (Fig. 1j) that were threaded through the chamber base and the bottom of each arm. We carried out the construction of the bases over a period of several months because the initial development

was an iterative process. However, if a user constructed the chambers directly from the designs provided in the present study, we estimate that construction could be completed in 2–4 weeks, depending on the daily person-power invested.

Chamber dome

We ordered clear acrylic domes that were 0.125-in (3 mm) thick with a height of 10 in (254 mm), a diameter of 20 in (508 mm), and a 0.375-in (10-mm) flange along the circumference to be affixed to the chamber bases during incubations (Fig. 1b). These dimensions yielded a chamber volume of 34.2 L. We modified the domes to create a fluid-tight seal when affixed to the bases, and to accommodate ports through which to take water samples during incubations. To create a fluid-tight seal, we added rubber trim to the flange at the bottom of the domes (Fig. 1k). Trim was 0.25 in (6 mm) wide by 0.5 in (13 mm) high and was cut to a length equal to the circumference of the domes. We applied the trim using non-toxic waterproof sealant. We installed sampling ports by tapping a threaded hole through the wall on opposite sides of the domes. We then screwed two threaded female luer connections directly through the domes (Fig. 1l). During deployment, a one-way stopcock with male-to-female luer connection was affixed to each of the female luer connections (Fig. 1m). The stopcock allowed the users to open and close the sampling ports as needed. At the apex of each dome, we also installed a drain plug to ease the manipulation of the domes while underwater (Fig. 1n). The drain plugs were 1-in (25-mm) boat drain plugs that were installed using machine screws and a 1-in (25-mm) diameter vulcanized fiber washer to prevent leakage around the installation point. Depending on current velocities and chamber specifications, this drain plug may not be necessary for all users.

Recirculating pumps

Each chamber also required a recirculating pump to successfully maintain a constant flow velocity and mix the water column in the chambers during incubations (Fig. 2a, Table 2; *see* Supporting Information Fig. S1 for imagery of individual component pieces). We used a recirculating pump constructed from a battery-powered 6-V water pump (flow rate = 1 L min^{-1}, flow velocity = 0.45 m s^{-1}) in a watertight PVC casing. The casing consisted of three PVC pieces: a 1.5-in (38-mm) diameter PVC pipe, a 2-in (508 mm) diameter PVC pipe, and a 1.5-in. (38-mm) by 0.75-in (19-mm) bushing reducer. The smaller end of the bushing reducer was threaded, so we stripped the threading using a 0.75-in (19 mm) hole saw bit. Then, we installed the pump into the end of the bushing

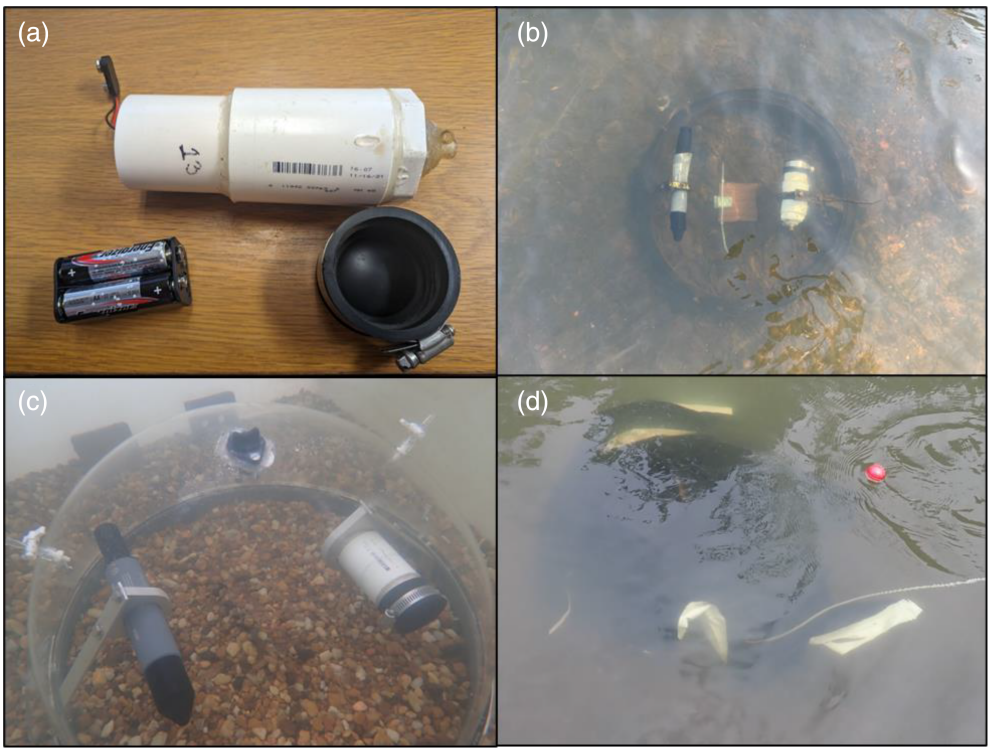

Fig. 2. Images of the recirculating pump and chamber incubations. (**a**) Partially assembled recirculating pump with battery casing and rubber end cap. (**b**) Initial data logger and pump deployment, showing from left to right: dissolved oxygen logger, light/temp logger, and recirculating water pump. (**c**) Fully sealed incubation chamber assembled in the lab. (**d**) Incubation chamber covered in ultraviolet-blocking tarp to conduct dark incubations in the field. Note the fishing bobbers used to mark the location of the chamber in the upper right-hand corner of panel (**d**) so it can be easily located prior to the incubation. Photos taken by J. W. Lopez and M. B. Lodato.

Table 2. A list of supplemental parts used to complete benthic metabolism measurements. Lengths and sizes are given in imperial units in parentheses, and in metric units in brackets. Images of each component part can be found in Supporting Information Fig. S1.

Category	Item	Origin	Cost
Recirculating pump	1.5-in [38-mm] PVC (10 ft) [305 cm]	Charlotte Pipe	$12.78
	2-in PVC [51 mm] (10 ft) [305 cm]	Charlotte Pipe	$17.74
	2-in [51-mm] PVC flexible cap	Fernco	$4.36 each
	1.5-in × 0.75-in [38 mm × 19 mm] PVC bushing reducer	Charlotte Pipe	$2.59 each
	DC-DC buck converter	BULVACK	$12.89 (pack of 10)
	6-V battery holder	LampVPath	$46.49 (pack of 3)
	6-V water pump	LightObject	$12.50 each
Data logger	HOBO Dissolved Oxygen Logger	Onset Computer Corporation	$1395.00
	HOBO 64K Pendant Temperature/Light Logger	Onset Computer Corporation	$105.00
	HOBO Waterproof Shuttle	Onset Computer Corporation	$325.00
	PME miniPAR Logger with USB connection cable	Precision Measurement Engineering	$2326.00
Anchoring grid	0.5-in [13-mm] mesh × 4-ft × 25-ft [122-cm × 762-cm]	Everbilt	$89.61 each
Dark incubation supplies	100% Ultraviolet-blocking shade cloth (24-ft × 10-ft) [762-cm × 305-cm]	Farm Plastic Supply	$41.00
	3-ft [91-cm] Cable ties	Commercial Electric	$14.41 (pack of 15)

using waterproof sealant. Before assembling the pump housing, we soldered the output terminals of a DC-to-DC buck converter to the electrical leads of the pump. We then soldered the input terminals to the leads of a snap connector for a 6-V battery holder. The battery holder held four AA batteries (1.5 V each). Once the converter and battery connections were installed, we placed the assembly inside the larger PVC pipe and sealed the bushing to the pipe using waterproof sealant. We sealed the smaller PVC pipe to the end of the larger one to complete the housing. Each housing was paired with a rubber end cap that could be affixed to the open end of the housing using a low-pressure clamp-on connector. With the caps installed, the pump housings were watertight.

Procedures

The procedures described below are based on a deployment in the Sipsey River, an undammed, fifth-order stream in western Alabama, USA. The Sipsey is an alluvial river with primarily sand and gravel sediments, low background nutrient concentrations, and extensive wetland floodplains (Atkinson et al. 2019). Like other southeastern US streams, the summer and autumn months are the periods of lowest flow, highest temperatures, and the greatest amount of biological activity (Benke et al. 2000; Atkinson et al. 2019). Our benthic chambers were designed specifically to be deployed under low flow conditions in alluvial sediments, but the design could be adapted for use in streams with other geomorphic characteristics.

Deployment

The first step in the deployment process is the installation of the chamber base into the stream bed at the study site. This requires the users to excavate the benthic sediment and refill the center of the chamber base with that sediment. The weight of the sediment pressing against the interior and exterior of the base then anchors the base in place at the location of installation. To strengthen the anchoring effect of the sediment in the bases, we attached a grid of galvanized steel hardware cloth with 0.5-in (13-mm) mesh size to the bottom of each base. We secured the grid by wrapping multiple 3-ft (91-cm) standard cable ties (Table 2) in a closed circle around the entire circumference of the base; we laced the cable ties through the grid and locked them in place flush against the exterior surface of the base. In softer, sandy, or muddy stream beds, excavation may not be necessary, and chambers may be pressed directly into the sediments similar to those in Roth et al. (2019)—although we have yet to test this method of installation.

To facilitate the excavation process, we used a 24-in by 24-in (610-mm by 610-mm) square steel brace with 10-in (254-mm) high sides produced using scrap sheet metal to prevent backfilling during excavation. We placed the brace on the stream bed at the desired location, then began excavating sediment using shovels. We excavated to a depth of ~ 20 cm, which was sufficient to place the chamber bases in a position where the acrylic lips at the top of the bases were nearly flush with the sediment surface (Fig. 2b,c). We sieved the excavated sediment into large plastic bins and removed macrofauna—mainly bivalves—that were trapped by the sieves. We chose to sieve the sediment and remove macrofauna for two reasons: first, to prevent undue stress or mortality to state-threatened and federally endangered freshwater mussels that are found at

the study site during portions of this study that involved concentrated solute injections (*see* Assessment section), and second, because this removal was a necessary step for additional field experiments that we conducted later in the field season. Once in position, we dumped the excavated sediment back into the steel brace, both inside and around the exterior of the chamber bases and removed the steel brace. Following this initial deployment, we allowed the chamber bases to set for at least 2 weeks to allow the benthic microbial and biofilm communities to return to equilibrium. Once installed, the bases can remain in situ for weeks to months without substantial maintenance, although extreme high-flow events might loosen or dislodge them.

Incubations

To conduct incubations, we deployed a series of data loggers (Table 2). We used a HOBO Dissolved Oxygen (DO) Data Logger (U26-001; Onset Computer Corporation) to monitor DO concentrations. The logger allows the continuous monitoring of DO levels during an incubation at preset time intervals. We used a HOBO Pendant Temp/Light 64 K Data Logger (UA-002-64) to simultaneously monitor light intensity. To launch the loggers prior to taking measurements and read out the data at the end of the incubations, we used a HOBO Waterproof Shuttle (U-DTW-1).

We powered on a recirculating pump and launched a DO logger, then placed them into the appropriate holsters (Fig. 2b). We also affixed a Pendant Light/Temp logger to a clay tile and placed it at the center of the chamber (Fig. 2b). However, benthic metabolism is sensitive to changes in photosynthetically active radiation (PAR), not necessarily light intensity because PAR becomes saturated at high light intensity. To account for this nonlinearity, we deployed a PME miniPAR PAR logger (Precision Measurement Engineering) inside an extra calibration chamber during each set of incubations. We used these calibration chambers to generate an asymptotic curve estimating PAR from light intensity (Long et al. 2012). Once the pump and necessary loggers were in place, we affixed the chamber domes to the buried bases (Fig. 2c). We submerged the domes and inverted them to remove air bubbles, moved them into place over the bases, and then sealed them to the bases with three acrylic brackets (Fig. 1o). We affixed these brackets to the machine screws protruding from the acrylic lip of the chamber base using six wingnuts (Fig. 1p). Once sealed, we closed the drain plugs and sampling ports to completely isolate the chamber environment (Fig. 2c).

To measure metabolism, we used 5-ft by 5-ft (152-cm by 152-cm) square tarps cut from 100% ultraviolet-blocking shade cloth to create dark incubation conditions (Fig. 2d; Table 2). We affixed the tarps over the chambers using a series of 3-ft (91-cm) standard cable ties. The exclusion of light halts primary production, allowing for the calculation of ER. Then, we removed the tarp, allowing primary production to resume and enabling the calculation of net ecosystem productivity (NEP)—the sum of gross primary productivity (GPP) and ER. The duration of the dark and light incubations depends on the goals and conditions of the study.

Assessment

Experimental design

To evaluate the functionality of our chamber design, we installed the chambers from 1 to 2 July 2024, allowed them to equilibrate, then conducted a two-part field experiment from 12 to 23 August 2024. The first part of the experiment was a performance test where we injected a conservative tracer into each chamber to quantify solute behavior inside the chambers in terms of mixing and retention. The second part of the experiment was a proof-of-concept test where we quantified ecosystem metabolism and performed nutrient additions across an example stream reach. We conducted all analyses in R v4.4.2 (R Core Team 2024).

The study reach was a ~ 50-m reach of a shallow run of the Sipsey River with gravel and sand substrate. We installed all 40 chambers along a series of 20 lateral transects spaced ~ 2 m apart. We installed two chambers ~ 2.5 m apart along each transect. Due to obstructions such as large wood and shallow depth, many chambers had to be moved slightly from their intended installation points. We assigned each chamber a unique identifying number (1–40) from upstream to downstream, with the most upstream chamber as number 1 and the most downstream chamber as number 40.

Performance testing: Solute dynamics

Methods

We conducted the performance testing portion of the experiment on 12–13 August 2024. We injected a conservative tracer (NaCl) into each metabolic chamber and recorded raw electrical conductivity at 1-min intervals using a HOBO Fresh Water Conductivity Data Logger (U26-001), as conductivity is roughly proportional to NaCl concentration. We converted electrical conductivity to specific conductance (SC) at 25°C using the equation

$$\mathrm{SC} = \frac{\mathrm{EC}}{1 + \alpha \times (T - 25)}$$

where α is the temperature coefficient, T is the observed temperature at the time of measurement, and $\alpha = 0.02$ (USEPA 1982). Average background SC in this portion of the Sipsey River in the late summer is around 100 μS cm^{-1} (Atkinson et al. 2019).

We placed a conductivity logger at the sediment surface in each chamber, allowing each logger to record for ~ 5–10 min before and after we sealed the chambers. We used these logger values to determine background SC levels for each incubation. Then, we increased SC by injecting 100 mL of 5% w/v NaCl solution. We injected the chambers in random order as

assigned by a random number generator. We also placed conductivity loggers in the stream to track ambient SC levels during both days of the experiment.

We quantified solute dynamics based on the assumption that two processes would dictate conductivity following the tracer injection: first, there would be an initial spike and rapid decline in SC as the solution became evenly mixed within the chamber; then SC would decline more gradually as it approached an asymptote. To model these dynamics, we first corrected for background SC using the values recorded at the beginning of each incubation. We then truncated the data for each incubation to remove the background readings, so that we modeled only the asymptotic decline in SC values following the initial spike. We fit an asymptotic decay model for each chamber incubation:

$$SC_t = \frac{-A \times t}{B + t} + C$$

where SC_t is background-corrected SC at time t, A is the scaling coefficient describing the initial, maximum rate of decline in SC_t, B is the half-saturation constant describing the rate at which SC_t approaches its asymptote, C is the asymptote of SC_t as t increases, and t is the incubation time in minutes. We fit an asymptotic decay curve for each chamber using the base R function *nls* and quantified goodness of fit using coefficients of determination (R^2).

Three days after completing the tracer injections, on 16 August 2024, we use a flow meter to measure near-bed flow velocity immediately adjacent to the upstream edge of each chamber to assess variation in the local hydraulic environment across the experiment (mean = 0.20 m s^{-1}; range = 0.06–0.41 m s^{-1}). Flow velocities at the outlet aperture of the recirculating pumps within each chamber were approximately 0.45 m s^{-1}, but the velocity of water coming from the pump will be attenuated by viscous drag and dispersion with distance from the outlet. Thus, we assume that flow velocities within the chambers fall within the range of the natural benthic conditions at our site during the experiment. We used the flow velocity measurements to test whether near-bed velocity was correlated with the parameter estimates of the asymptotic decay models describing solute dynamics inside the chambers.

Results and conclusions

Ambient SC (mean ± SD) was 109.9 ± 0.8 μS cm^{-1} on 12 August, and 115 μS cm^{-1} on 13 August. The magnitude of the initial spikes in SC was highly variable across chambers (Fig. 3). While it is difficult to know the definitive cause of this variation, we find the most likely explanation is that the timing of the true peak of SC did not perfectly align with the logging interval. For example, some loggers may have taken a measurement immediately before the injection, allowing a full minute of solute mixing to occur prior to recording another value; other loggers may have recorded a value immediately after the injection and captured a massive spike prior to mixing. This suggests that a more synchronized approach where the injection is timed to match the logging interval, or simply an increased logging frequency, might be useful for capturing the magnitude and timing of the initial spike in SC more precisely.

Of the 40 chambers, 39 followed the expected asymptotic decline in SC values over the course of the incubations (Fig. 3). We excluded the anomalous chamber (ID 36) from further analysis because it was clear that this chamber was either not retaining or not mixing solutes in the same way as the others. For the remaining chambers, asymptotic decay models provided an excellent fit, with a mean (± SD) R^2 value of 0.93 ± 0.06 (Supporting Information Table S1). Asymptotic decay models showed that SC tended to decay more quickly towards the asymptote, and that the asymptote tended to be closer to background SC, as near-bed flow velocity around the chambers increased (Fig. 4). The scaling coefficient A tended to decrease monotonically with near-bed flow velocity ($F_{1,37} = 5.6$, $p = 0.023$, $R^2 = 0.13$, log $-y = -2.98x + 7.60$; Fig. 4a), while the half-saturation constant B tended to increase ($F_{1,37} = 16.4$, $p = 2.55 \times 10^{-4}$, $R^2 = 0.31$, log $y = 7.29x - 0.91$; Fig. 4b). The baseline SC response, or asymptote, C, tended to become lower and closer to background SC as flow velocity increased ($F_{1,37} = 8.7$, $p = 0.006$, $R^2 = 0.19$, log $y = -3.31x + 7.78$; Fig. 4c).

Based on the data presented here, our benthic chamber design performed well, other than chamber 36. The open-bottom design tended to retain solutes for longer when flow velocities were low. This is presumably because high flow velocities can create turbulent flow paths and pressure gradients, leading to exchange between surface waters and the hyporheic zone (Gadeken et al. 2023). Covariation of the half-saturation constant B with flow velocity indicates that such hyporheic exchange caused solutes to diffuse more quickly out of the chambers. Interestingly, the scaling coefficient A decreased with increasing flow velocity. We think the most likely cause for the opposite relationships that A and B had with flow velocity is that SC declined rapidly enough in high-velocity chambers that by the time the electrical conductivity loggers made their first readings, SC values had already declined to a greater extent than in the low-velocity chambers, creating an apparent depression in the initial rate of decline. In the chambers where SC reached half-saturation quickly, we suspect that hydraulic forces—presumably a pressure gradient—created by rapidly flowing water around the slower-moving water in the chambers may have caused the hyporheic zone to mix with the surface water that was originally enclosed in the chamber. This issue may be further exacerbated by the porous sand and gravel sediments in our system. It is possible that during the installation process, finer sediments may have been lost from the chambers as we dumped the excavated sediments back into the installation locations. The combination of a pressure gradient and more porous sediments would account for the rapid diffusion of solutes (Whitaker 1986). We suggest

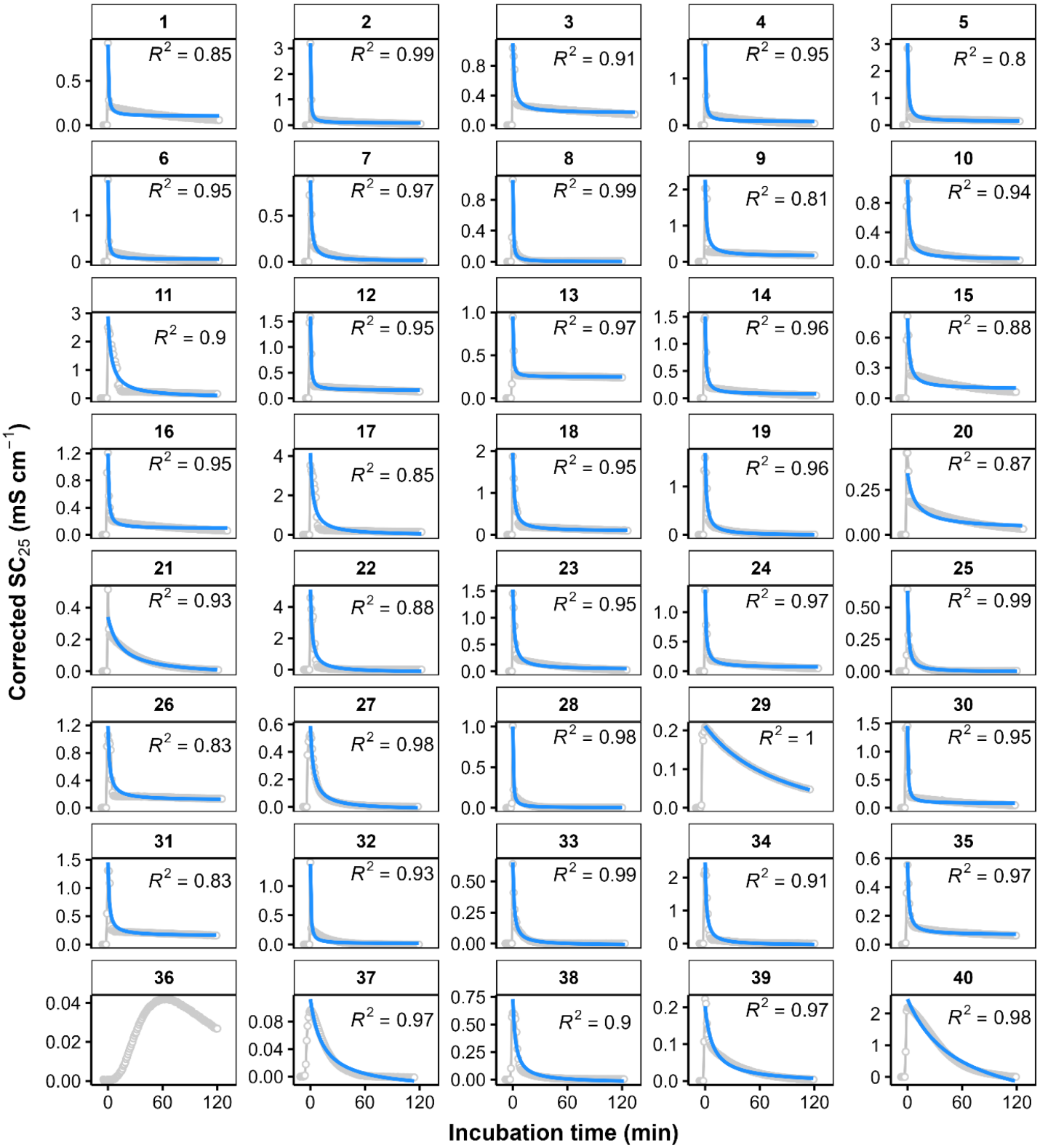

Fig. 3. Asymptotic decay curves showing solute dynamics during a conservative tracer (5% NaCl w/v) injection (SC_{25} = specific conductivity at 25°C). Numbered panel labels show the unique numeric identifier for each chamber. The *y*-axes are scaled individually because the initial SC_{25} value depends strongly on the timing of the first conductivity logger reading value relative to the tracer injection.

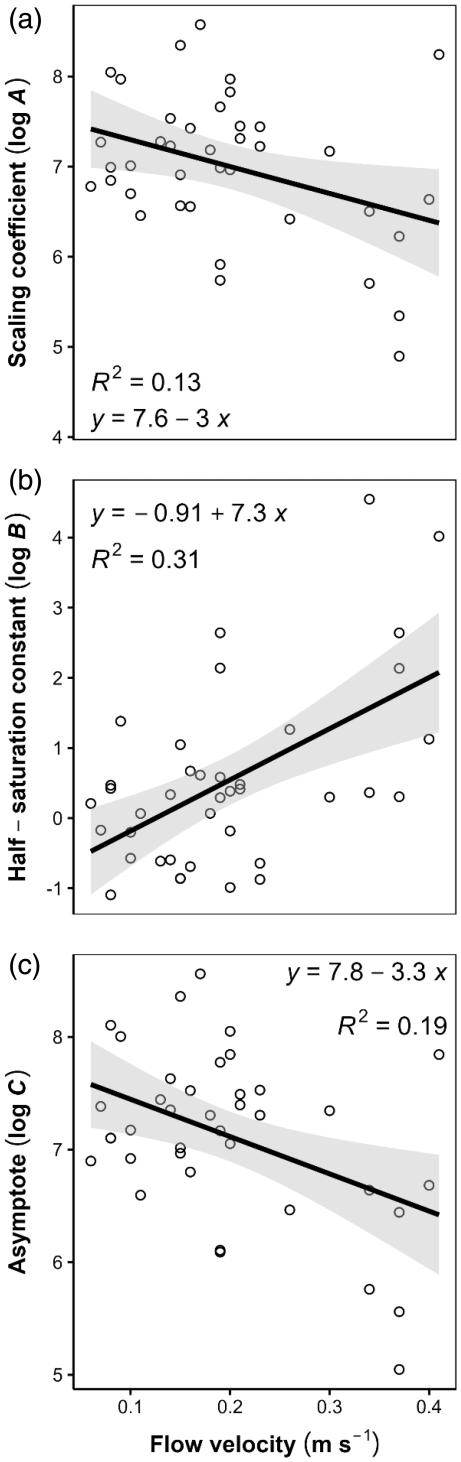

Fig. 4. Response of (**a**) the scaling coefficient *A*, (**b**) the half-saturation constant *B*, and (**c**) the regression asymptote *C* to near-bed flow velocity. Shaded confidence bands represent 95% confidence interval. Note the log-transformed *y*-axes.

that one of the limitations of our open-bottom design is likely related to complex hydraulic patterns that are caused by high flow velocities and potentially the loss of fine sediments during installation. As with all benthic chambers, our design can only capture a cross section of the natural heterogeneity that is inherent to streams, including hydraulic, physical, and biogeochemical factors that impact ecosystem function.

Proof of concept: Benthic metabolism and nutrient additions

Methods

To demonstrate the utility of our chambers for quantifying biogeochemical rates, we conducted a two-part field study on 19–23 August 2024. We conducted a series of incubations where we simultaneously (1) measured benthic metabolism using the incubation procedures described above and (2) injected nutrient solutions of dissolved nitrogen (N) and phosphorus (P) to demonstrate the potential usefulness of the chambers for quantitative studies of nutrient dynamics.

Benthic metabolism

To quantify benthic metabolism, we assembled each chamber sequentially. We conducted a 4-h incubation for each chamber—dark incubations for 2 h, followed by light incubations for 2 h. We conducted 10 incubations per day, in a randomly selected order ($N = 40$). We calculated ER and GPP using time series O_2 concentration data collected at one-minute intervals using the DO loggers during each incubation. We split the resulting data set into light and dark incubation periods, then conducted local linear regression analyses on the resulting O_2 flux curves (package LoLinR; Olito et al. 2017). Local linear regression reduces bias and increases accuracy in the estimation of monotonic biological rates by identifying the slope of the most linear subset of a time series, reducing the need for potentially subjective measures such as manual data truncation (Olito et al. 2017; Roth et al. 2019). The LoLinR package (function rankLocReg) requires the user to set a minimum proportion (alpha) of the total number of observations in the time series (N) to be used in the analysis. At minimum, alpha $\times$ $N \geq 15$. However, data may still require manual truncation in the presence of saturation effects or when noise or sensor errors occur near the middle of an incubation (Lopez et al. 2025). In such cases, the problematic portion of the time series should be removed, and the analysis should be rerun. The slopes of the O_2 fluxes, standardized for chamber volume and surface area (g O_2 $m^{-2} h^{-1}$) represent ER in dark incubations and NEP in light incubations. Then GPP is then calculated as NEP + ER. During the incubations, we also constructed curves of DO, temperature, and light intensity over time because temperature and light directly impact benthic metabolism. However, light intensity scales nonlinearly with PAR, so we developed an asymptotic regression model to predict PAR from light intensity values using nonlinear least squares regression (Long et al. 2012; package drc; Ritz et al. 2015).

We recorded a GPS point for each chamber using a handheld Garmin GPSMAP 66st (Garmin Ltd) and then used kernel density interpolation with boundaries to create site-level

geospatial models of ER, GPP, and NEP across the study reach. We cross-validated the resulting models using the leave-one-out method to quantify their accuracy in ArcGIS Pro v3.0.3 (Environmental Systems Research Institute).

Nutrient addition

At the conclusion of the dark incubations, we injected nutrient solutions to demonstrate how the chambers might be used to study nutrient dynamics. Average background nutrient concentrations at the same study site in 2023 were 12.4 μg N L^{-1} and 3.98 μg P L^{-1} (N : P = 6.89) (Lopez et al. 2025). We aimed to elevate background concentrations by injecting solutions of dissolved N (NH_4Cl at 0.614 g L^{-1}) and P (KH_2PO_4 at 0.227 g L^{-1}) into the chambers through the sampling ports created by the stopcocks attached to the exterior of each dome. We injected relatively more N due to the higher background concentrations of N. We injected these solutions into the chambers to create four nutrient addition treatments: an N addition treatment (10 mL N solution), a P addition treatment (10 mL P solution), an N + P treatment (10 mL N solution +10 mL P solution), and a control treatment (10 mL stream water). We assigned treatments randomly. We initially aimed to achieve $n = 10$ for each treatment; however, on the last day of the experiment, a bottle of P solution broke during transport to the field site, and so one P addition and one N + P addition were run as control incubations ($n = 10$ for N, $n = 9$ for P, $n = 9$ for N + P, $n = 12$ for control). During the light incubation, we sampled ambient water nutrient concentrations by opening both sampling ports and withdrawing 25 mL of water from the interior of each chamber using a plastic, luer-locking syringe that we attached directly to the sampling port. We opened both ports to allow a small volume of stream water to replace the sampling volume, rather than create a pressure gradient that could pull deoxygenated porewater from the hyporheic zone into the chamber. We sampled nutrient concentrations at 5 (t_1), 10 (t_2), 20 (t_3), 40 (t_4), 60 (t_5), 90 (t_6), and 120 (t_7) min after injection. After taking each sample, we carefully removed the syringe from underwater so that the sample would not be displaced by stream water, and we filtered the sample through a 0.7 μm glass fiber filter (GF/F). We analyzed nutrient concentrations (μM) using a Seal AQ300 discrete analyzer (Seal Analytical). We removed seven data points that were ≥ 3 standard deviations from the mean concentration of each nutrient (N: $n = 3$; P: $n = 4$). The most likely explanation for these outliers is that nutrients were slow to mix after injection into their respective chambers, although we cannot rule out analytical error. Regardless, these points represented a small proportion of the original total sample size ($N = 560$), so their exclusion did not unduly impact the results of the experiment.

We determined nutrient removal rates by analyzing temporal trends in the log-transformed concentrations of each nutrient for each chamber using the following multiple linear regression model:

$$\mathrm{lm}(\log \mathrm{Concentration} \sim \mathrm{Nutrient} \times \mathrm{Time} \times \mathrm{Chamber}).$$

We isolated the slope of the "Time" effect for each chamber using the R function *emtrends* (package *emmeans*; Lenth 2023). The resulting slopes represent exponential decay rate constants (k) for the removal of each nutrient in all chambers. For simplicity, we refer to k as the nutrient removal rate. We then compared the nutrient removal rates for N and P across all four nutrient addition treatments using a Kruskal–Wallis test because the slopes lacked homogeneity of variance (Levene test: $F_{7,72} = 4.1$, $p = 0.001$). We used a post hoc Dunn test with Benjamini-Hochberg-adjusted p-values to identify pairwise differences among treatments for each nutrient.

Results and conclusions

Benthic metabolism

We successfully isolated linear slopes from DO curves in 39 dark incubations and in all 40 light incubations. In the dark incubations that we used to calculate ER, the curves were mostly linear throughout the 2-h incubation (Fig. 5). Chamber 28 was the only incubation where we could not isolate an ER slope because DO concentrations remained largely stable during this dark incubation. In the light incubations, some curves—especially those in shallower portions at the downstream end of the study reach, for example, chambers 36–40—created DO saturation effects as the incubations progressed (Fig. 5). In these cases, we manually truncated the datasets to remove the asymptotic portion of the curves. Mean (± SD) ER was -0.09 ± 0.05 g O_2 m^{-2} h^{-1}, GPP was 0.31 ± 0.25 g O_2 m^{-2} h^{-1}, and NEP was 0.21 ± 0.24 g O_2 m^{-2} h^{-1}.

Kernel density interpolation showed hotspots of ER in chambers positioned in deeper areas near the center of the study reach (Fig. 6a). GPP showed the opposite pattern and was highest at the downstream end of the study reach where water was shallower and flow velocity was faster, although GPP hotspots were less clearly defined (Fig. 6b). NEP showed a similar spatial pattern to GPP, presumably because GPP had a larger range of values than ER (Fig. 6c). Root-mean-square values for the cross-validated models were 0.0058 for ER, 0.026 for GPP, and 0.024 for NEP. Mean cross validation error was -1.4×10^{-3} for ER, 4.2×10^{-4} for GPP, and -9.8×10^{-5} for NEP. While these cross-validation errors are relatively low compared to the metabolic rates we measured, the model may be disproportionately influenced by some data points due to the uneven distribution of the chambers across the stream reach. The presence of several obstructions, mainly large wood and shallow portions of the stream, caused us to adjust the installation locations away from the original equidistant transects. Also, the handheld GPS unit we used has a reported accuracy of 2.14–3.53 m (US Forest Service, NTDP GPS Receiver Horizontal Accuracy Reports, https://www.fs.usda.gov/database/gps/mtdcrept/accuracy/index.htm), which could also create some uncertainty in the spatial distribution of the

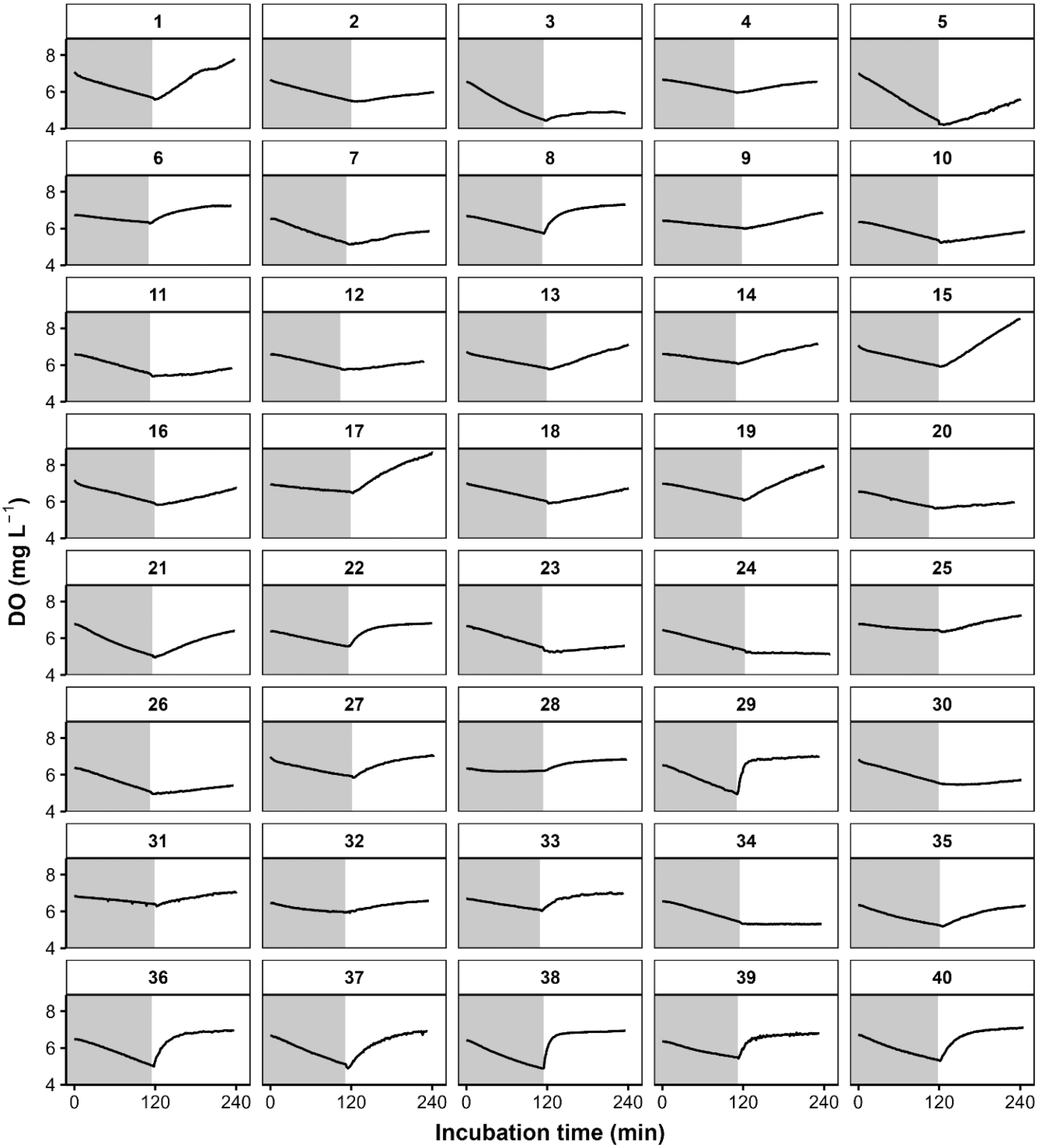

Fig. 5. Dissolved oxygen (DO) curves from the metabolism experiment. Numbered panel labels show the unique numeric identifier for each chamber. Shaded portions on the left-hand side of the panels represent dark incubation conditions. Unshaded portions to the right represent light incubation.

mapped chambers. The result is that more isolated data points tend to have a stronger impact on the interpolated metabolic rates around them (Fig. 6).

Across all chambers, temperature generally remained stable or increased at a slow rate (mean ± SD = 0.22 ± 0.18° C h^{-1}) during the dark incubations, and then immediately began to

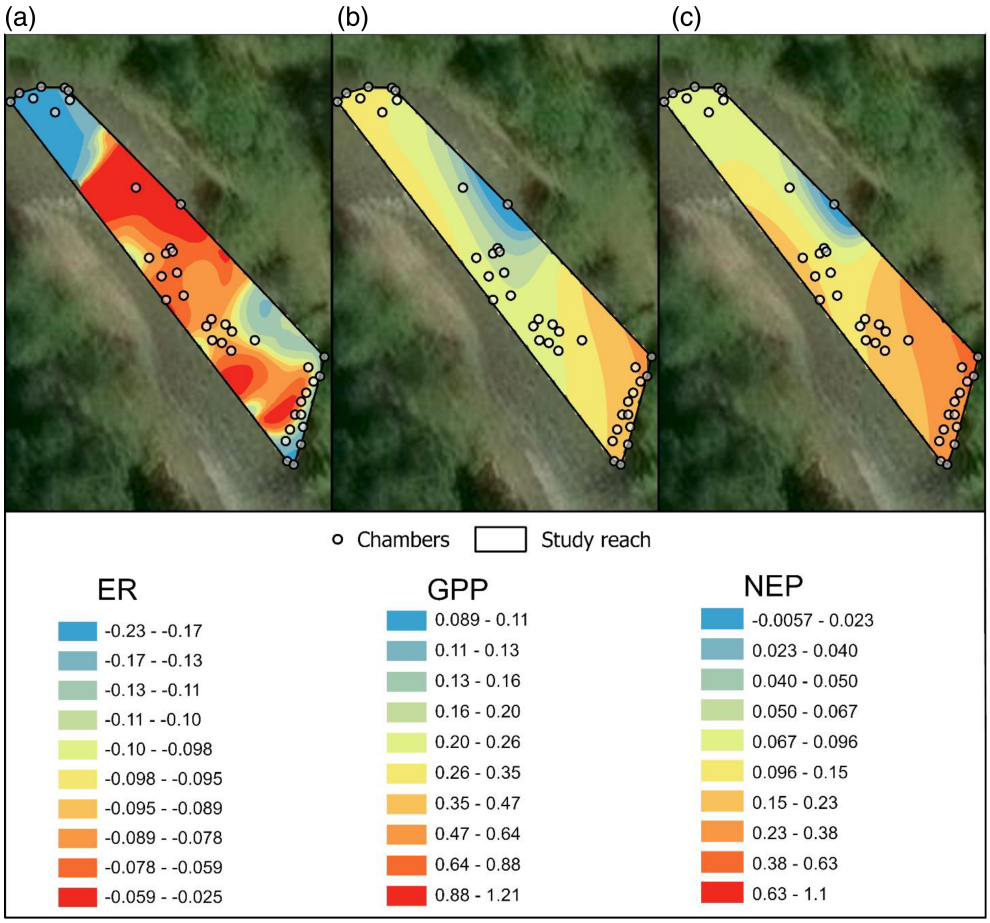

Fig. 6. Kernel density interpolation of (**a**) ecosystem respiration (ER), (**b**) gross primary productivity (GPP), and (**c**) net ecosystem productivity (NEP) in the experimental stream reach. Units for all three legends are mg O_2 m^{-2} h^{-1}. Note differences in the range of the scales.

rise at a faster rate (0.84 ± 0.49°C h^{-1}) during the light incubations (Supporting Information Fig. S2). Light intensity values remained at 0 during dark incubations, demonstrating the effectiveness of the ultraviolet-blocking tarps we employed, and then fluctuated widely during the light incubations with varying cloud cover and time of day (Supporting Information Fig. S3). We were able to estimate PAR from light intensity; however, the coefficient of determination was relatively modest ($R^2 = 0.52$; Supporting Information Fig. S4).

Nutrient addition

We considered mean (± SD) nutrient concentrations in the control treatments at t_1 to be representative of background conditions in the chambers because they were not injected with nutrients (NH_4^+–N $= 0.915 \pm 0.264$ μM, soluble reactive phosphorus [SRP] $= 0.353 \pm 0.0422$ μM). On average, NH_4^+–N concentrations spiked by 190% at t_1 in the N addition treatment relative to the controls, and by 151% in the N + P additions. The SRP concentrations spiked by an average of 56% in the P additions and 42% in the N + P additions.

In the control treatments, NH_4^+–N removal rates were more negative than SRP removal rates ($z = 3.0$, $p = 0.014$) (Fig. 7). This contrast suggests the study site may be N-limited and undergo net benthic N removal and/or uptake under ambient conditions. In the N additions, NH_4^+–N removal rates were more negative than the control treatment ($z = -2.9$, $p = 0.017$), and SRP removal rates remained similar to those in the control treatments, as expected ($z = -0.7$, $p = 0.672$) (Fig. 7). Conversely, in the P additions, SRP removal rates were more negative than the controls ($z = -2.8$, $p = 0.017$), while NH_4^+–N removal rates remained similar to the controls ($z = -0.7$, $p = 0.672$) (Fig. 7). These steep removal rates in the injected nutrients may be attributed to increased rates of biological uptake or transformation, or to increased diffusion into the hyporheic zone—the rates of both mechanisms should increase with nutrient concentrations. Declines in P concentrations might also be related to adsorption, which can vary with the relative concentrations of specific elements such as Ca, or Fe, Al and their oxides (Reddy et al. 1999; Li et al. 2012). Finally, in the N + P additions, the slopes of the declines in both N ($z = 0.1$, $p = 1.000$) and P removal rates

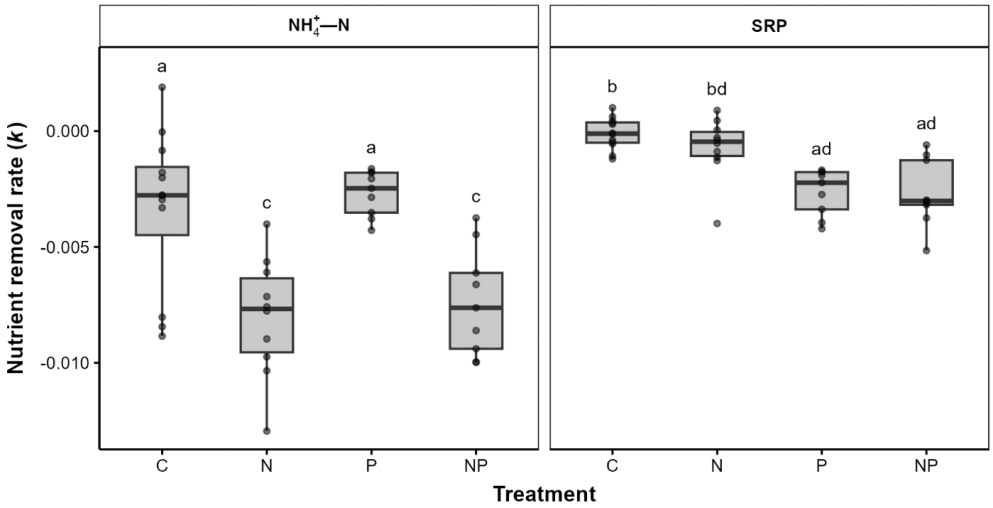

Fig. 7. Results of the nutrient addition test in the benthic chambers. Nutrient removal rates for ammonia (NH_4^+–N) and soluble reactive phosphorus (SRP) varied depending on which nutrient addition treatment was applied. Groups with shared letters cannot be statistically distinguished based on a Dunn test with Benjamini-Hochberg-corrected *p*-values ($\alpha = 0.05$).

($z = 0$, $p = 1.000$) were similar to those in the single nutrient addition treatments (Fig. 7).

Altogether, these results provide clear evidence of a detectable spike in nutrient concentrations during the additions we performed and demonstrate the usefulness of the chambers for calculating nutrient removal or uptake rates. Isolating the mechanisms responsible for nutrient removal from the chambers would require additional methodological steps, such as the simultaneous addition of a conservative tracer (rather than the separate tracer experiment we conducted above), or the use of stable isotopes for N, which would allow the user to disentangle biological uptake from physical removal mechanisms such as hyporheic exchange and adsorption.

Discussion

The novel benthic chamber design we have presented enables aquatic scientists to conduct new and innovative ecosystem experiments in streams. Specifically, we have demonstrated the capacity of this design to generate quantitative, spatially explicit estimates of ecosystem metabolism and to extrapolate them across the study stream reach. We also showed that the chambers can be used to experimentally test solute and nutrient dynamics. The ability to install the chambers in situ for a period of weeks to months allows for natural biogeochemical conditions to reestablish and for ecosystem processes to be isolated, thus providing a high level of experimental control to test mechanistic hypotheses.

To illustrate the experimental potential of these chambers, we conducted a separate experiment designed to answer questions relating to the ecosystem impacts of stream-dwelling animals using freshwater mussels (Bivalvia: Unionoida) (Lopez et al. 2025). In that study, we were able to quantify mussel-driven impacts on ER and GPP and isolate the ecophysiological and behavioral traits (i.e., horizontal and vertical movement) that were responsible for those impacts. Creative experimental designs could employ these chambers to answer similar questions with other large aquatic animals like fish, snails, or amphibians—although challenges related to the mobility of these taxa would require some ingenuity on the part of the users to resolve. Lopez et al. (2025) also highlights another key aspect of the chambers: their ability to accommodate benthic macrofauna. While historically overlooked, the biogeochemical impacts of animals are increasingly being recognized as key drivers of ecosystem function (Vanni 2002; Schmitz et al. 2014, 2018; Atkinson et al. 2017). Our chambers allow the users to assess the magnitude of freshwater animal-driven ecosystem function through experimental species additions or removals.

Of course, this chamber design is not without limitations. As discussed above, the tracer injection we performed indicated that chambers placed in fast-flowing areas did not retain the conservative tracer for long. While we did not account for solute loss via diffusion through the open chamber bottom in our nutrient addition test, one could do so mathematically by conducting the tracer and nutrient additions simultaneously (Covino et al. 2010; Baker and Webster 2017). This would allow for the quantification of specific nutrient cycling pathways such as areal uptake. It is also likely that much of the fine sediment and particular organic matter that were initially present at the installation site for each chamber were lost during the sieving portion of the excavation. While some of this loss should be replenished naturally during the 2-week equilibration period following installation, it is possible that the

installation process altered sediment redox profiles, thereby altering the biogeochemical rates within the chamber. The quantity of this potential loss could be measured by sampling the organic matter content and sediment size distributions of the benthic zone outside of the chambers and comparing the data to the same properties within the chambers. It is difficult to know exactly how the loss of fine particles could affect the results of our experiments, but it is worth considering for future use. Yet, it is perhaps more important to place the benefits and limitations of this design in the context of the trade-offs it presents in relation to other popular benthic chamber designs.

The main benefits that the present chambers have compared with portable designs such as those popularized by Dodds and Brock (1998) and Rüegg et al. (2015) are (1) their capacity for installation directly into the stream bed—which allows for both the real-time measurement of ecosystem processes without removing sediments from the benthic zone and the generation of spatially explicit data, and (2) their large size, allowing for the accommodation of macrofauna. However, users should take care to optimize the spatial distribution of their chambers across the study site, so as to prevent the occurrence of isolated, high-leverage data points when performing spatial data interpolation. The size of these chambers also creates some of their main limitations. First, the stream being sampled must be of sufficient depth to accommodate the height of the dome once the chambers are sealed. This of course means that the chambers cannot be deployed in very small streams and can also create data gaps if the margins of a study reach are shallow. These gaps can be seen around the boundaries of the geospatial metabolism models we generated in the present study. The result is that shallow banks within a given stream reach may be missed due to the size limitations of the chambers. The size and shape of our chamber design also increase the chamber-volume to sample-area ratio. As a result, biogeochemical rates must be fast enough to be detected in the 34.2 L of water that are contained in each chamber, whereas small, portable chambers are likely better suited for detecting much smaller fluctuations. However, the size, or even the shape, of our in situ chamber design could also be modified based on the question or system being tested and the aims of the study that uses them. Modifications could include decreasing the height for use in shallower streams or changing the aspect ratio to minimize the volume to sample-area ratio.

Additional trade-offs include limitations on flow manipulation imposed by the self-contained pump design and the cost of production. Flow inside the present chambers cannot be manipulated during an experiment and is not unidirectional whereas portable, rectangular chambers can use propellers to drive unidirectional flow, and flow velocity can be manipulated by adjusting a power supply box connected to the motor (Rüegg et al. 2015). Larger diameter propellers are also more energy efficient and can achieve higher flow velocities than pumps. Using an external power supply also prevents the power source from heating the chamber environment and consequently altering metabolic rates. However, heating in our experiment appeared to be primarily a result of light penetration, as heating occurred at a nearly 4× faster rate in light incubations. On the other hand, the large volume of water contained within our chambers likely minimizes the heating effect due to the low surface area-to-volume ratio for the dissipation of heat. In any case, the completely self-isolated nature of the chambers we designed precludes the use of an external power source—although, a more technologically advanced power source could allow users to manipulate the speed of the pump remotely. Additional studies would be needed to truly understand the impact of our pump design on the estimation of biogeochemical rates. An ideal next step would be to map the velocity profiles of flow within the chambers in a controlled environment, using tools such as acoustic Doppler velocimetry. This would allow for a direct comparison between flow rates within the chambers and ambient flow.

Comments and recommendations

The chamber design we have presented is not meant to compete with, nor replace other well-established portable designs, but to provide a complementary alternative that allows users to ask and answer different questions at larger scales. There is no ideal chamber design that fully replicates natural environmental conditions, so decisions regarding the specific type of chamber and custom modifications to their designs must be made by individual users. For those seeking a fine-scale understanding of nutrient dynamics or specific biogeochemical pathways in benthic biofilms, perhaps a portable chamber is best. Portable chambers also allow for a complete seal, which is not possible using our design. But for those seeking to conduct larger-scale ecosystem experiments in situ with reduced sediment disturbance, especially involving larger organisms, our design represents a new approach to answering a broad variety of questions. For example, we have already begun testing the applicability of this design to a number of other questions related to consumer-driven nutrient dynamics, denitrification, biofiltration, and bioturbation (M.B. Lodato, T.C. Michael, L.M. Morris, unpublished; Lopez et al. 2025). Further, the ability to contain organisms within the chambers we have presented allows for the potential to test biodiversity–ecosystem function relationships (Loreau et al. 2001), or artificial heating elements could be employed to test climate-related hypotheses.

The questions that may be asked using the present chamber design are diverse, but we have only presented their applicability in one alluvial sand-gravel system. We encourage those who are interested in employing some version of this design in systems with other geomorphic characteristics to do similar methodological tests to those conducted here and modify the design if necessary. While we constructed these chambers for

use in streams, they could also be deployed in a lake or pond environment with little modification. Ultimately, we believe that these chambers have great potential to improve the existing understanding of freshwater ecosystem processes and provide a high level of manipulative control among field experiments. We encourage those who may be interested in employing such a design to develop their own prototypes based on our designs and, if necessary, adapt the methods to their chosen systems to advance the field of aquatic ecology, especially in streams.

Acknowledgments

We thank Pierce Austin, Taylor Kelley, and Kelton Verble for assistance in the field, and the Weyerhaeuser Company for granting us access to our study site. James Pugh and the University of Alabama College of Arts and Sciences Machine Shop cut the custom parts and performed the initial assembly of the chambers. Anne Bell conducted the nutrient analyses. We also thank Walter Dodds and an anonymous reviewer for helpful comments that improved the original manuscript. The National Science Foundation provided funding support for this project (DEB-1942707 and DBI-2305574).

Conflicts of Interest

The authors declare no conflicts of interest.

References

Atkinson, C. L., K. A. Capps, A. T. Rugenski, and M. J. Vanni. 2017. "Consumer-Driven Nutrient Dynamics in Freshwater Ecosystems: From Individuals to Ecosystems." *Biological Reviews* 92: 2003–2023. https://doi.org/10.1111/brv.12318.

Atkinson, C. L., B. C. van Ee, Y. Lu, and W. Zhong. 2019. "Wetland Floodplain Flux: Temporal and Spatial Availability of Organic Matter and Dissolved Nutrients in an Unmodified River." *Biogeochemistry* 142: 395–411. https://doi.org/10.1007/s10533-019-00542-z.

Baker, M. A., and J. R. Webster. 2017. "Conservative and Reactive Solute Dynamics." In Methods in Stream Ecology, edited by G. A. Lamberti and F. R. Hauer, 129–145. Cambridge: Elsevier.

Battin, T. J., S. Luyssaert, L. A. Kaplan, A. K. Aufdenkampe, A. Richter, and L. J. Tranvik. 2009. "The Boundless Carbon Cycle." *Nature Geoscience* 2: 598–600. https://doi.org/10.1038/ngeo618.

Benke, A. C., I. Chaubey, G. M. Ward, and E. L. Dunn. 2000. "Flood Pulse Dynamics of an Unregulated River Floodplain in the Southeastern U.S. Coastal Plain." *Ecology* 81: 2730–2741. https://doi.org/10.1890/0012-9658(2000)081[2730:FPDOAU]2.0.CO;2.

Bott, T. L., J. T. Brock, A. Baatrup-Pedersen, et al. 1997. "An Evaluation of Techniques for Measuring Periphyton Metabolism in Chambers." *Canadian Journal of Fisheries and Aquatic Sciences* 54: 715–725. https://doi.org/10.1139/f96-323.

Cole, J. J., Y. T. Prairie, N. F. Caraco, et al. 2007. "Plumbing the Global Carbon Cycle: Integrating Inland Waters into the Terrestrial Carbon Budget." *Ecosystems* 10: 171–184. https://doi.org/10.1007/s10021-006-9013-8.

Covino, T. P., B. L. McGlynn, and R. A. McNamara. 2010. "Tracer Additions for Spiraling Curve Characterization (TASCC): Quantifying Stream Nutrient Uptake Kinetics from Ambient to Saturation." *Limnology and Oceanography: Methods* 8: 484–498. https://doi.org/10.4319/lom.2010.8.484.

Dodds, W. K., and J. Brock. 1998. "A Portable Flow Chamber for *In Situ* Determination of Benthic Metabolism." *Freshwater Biology* 39: 49–59. https://doi.org/10.1046/j.1365-2427.1998.00256.x.

Dodds, W. K., A. M. Veach, C. M. Ruffing, D. M. Larson, J. L. Fischer, and K. H. Costigan. 2013. "Abiotic Controls and Temporal Variability of River Metabolism: Multiyear Analyses of Mississippi and Chattahoochee River Data." *Freshwater Science* 32: 1073–1087. https://doi.org/10.1899/13-018.1.

Duff, J. H., K. C. Stanley, F. J. Triska, and R. J. Avanzino. 1984. "The Use of Photosynthesis-Respiration Chambers to Measure Nitrogen Flux in Epilithic Algal Communities: With 2 Figures and 3 Tables in the Text." *SIL Proceedings, 1922–2010* 22: 1436–1443. https://doi.org/10.1080/03680770.1983.11897515.

Fuller, R. L., and J. B. Bucher. 1991. "A Portable Chamber for Measuring Algal Primary Production in Streams." *Hydrobiologia* 209: 155–159. https://doi.org/10.1007/BF00006927.

Gadeken, K. J., G. Lockridge, and K. M. Dorgan. 2023. "An In Situ Benthic Chamber System for Improved Temporal and Spatial Resolution Measurement of Sediment Oxygen Demand." *Limnology and Oceanography: Methods* 21: 645–655. https://doi.org/10.1002/lom3.10571.

Hall, R. O., Jr., M. A. Baker, C. D. Arp, and B. J. Koch. 2009. "Hydrologic Control of Nitrogen Removal, Storage, and Export in a Mountain Stream." *Limnology and Oceanography* 54: 2128–2142. https://doi.org/10.4319/lo.2009.54.6.2128.

Hall, R. O., M. A. Baker, E. J. Rosi-Marshall, J. L. Tank, and J. D. Newbold. 2013. "Solute-Specific Scaling of Inorganic Nitrogen and Phosphorus Uptake in Streams." *Biogeosciences* 10: 7323–7331. https://doi.org/10.5194/bg-10-7323-2013.

Hotchkiss, E. R., R. O. Hall, R. A. Sponseller, et al. 2015. "Sources of and Processes Controlling CO_2 Emissions Change with the Size of Streams and Rivers." *Nature Geoscience* 8: 696–699. https://doi.org/10.1038/ngeo2507.

Humphries, A. T., S. G. Ayvazian, J. C. Carey, et al. 2016. "Directly Measured Denitrification Reveals Oyster Aquaculture and Restored Oyster Reefs Remove Nitrogen at Comparable High Rates." *Frontiers in Marine Science* 3: 1–10. https://doi.org/10.3389/fmars.2016.00074.

Kellogg, M., J. Cornwell, M. Owens, and K. Paynter. 2013. "Denitrification and Nutrient Assimilation on a Restored Oyster Reef." *Marine Ecology Progress Series* 480: 1–19. https://doi.org/10.3354/meps10331.

Lenth, R. V. 2023. emmeans: Estimated Marginal Means, aka Least-Squares Means.

Li, Y., S. Yu, J. Strong, and H. Wang. 2012. "Are the Biogeochemical Cycles of Carbon, Nitrogen, Sulfur, and Phosphorus Driven by the 'FeIII–FeII Redox Wheel' in Dynamic Redox Environments?" *Journal of Soils and Sediments* 12: 683–693. https://doi.org/10.1007/s11368-012-0507-z.

Long, M. H., J. E. Rheuban, P. Berg, and J. C. Zieman. 2012. "A Comparison and Correction of Light Intensity Loggers to Photosynthetically Active Radiation Sensors: Comparison of Light Loggers and PAR Sensors." *Limnology and Oceanography: Methods* 10: 416–424. https://doi.org/10.4319/lom.2012.10.416.

Lopez, J. W., M. B. Lodato, and C. L. Atkinson. 2025. "Zoogeochemical Impacts of Freshwater Mussels on Stream Metabolism Are Mediated by their Ecophysiological and Behavioral Traits." *Freshwater Science* 44, no. 1: 31–44. https://doi.org/10.1086/733812.

Loreau, M., S. Naeem, P. Inchausti, et al. 2001. "Biodiversity and Ecosystem Functioning: Current Knowledge and Future Challenges." *Science* 294: 804–808. https://doi.org/10.1126/science.1064088.

Maranger, R., S. E. Jones, and J. B. Cotner. 2018. "Stoichiometry of Carbon, Nitrogen, and Phosphorus through the Freshwater Pipe." *Limnology and Oceanography Letters* 3: 89–101. https://doi.org/10.1002/lol2.10080.

Minshall, G. W. 1988. "Stream Ecosystem Theory: A Global Perspective." *Journal of the North American Benthological Society* 7: 263–288. https://doi.org/10.2307/1467294.

Olito, C., C. R. White, D. J. Marshall, and D. R. Barneche. 2017. "Estimating Monotonic Rates from Biological Data Using Local Linear Regression." *Journal of Experimental Biology* 220, no. Pt 5: jeb.148775. https://doi.org/10.1242/jeb.148775.

R Core Team. 2024. R: A Language and Environment for Statistical Computing. Vienna: R Foundation for Statistical Computing. https://www.R-project.org/.

Reddy, K. R., R. H. Kadlec, E. Flaig, and P. M. Gale. 1999. "Phosphorus Retention in Streams and Wetlands: A Review." *Critical Reviews in Environmental Science and Technology* 29: 83–146. https://doi.org/10.1080/10643389991259182.

Ritz, C., F. Baty, J. C. Streibig, and D. Gerhard. 2015. "Dose-Response Analysis Using R." *PLoS One* 10: e0146021. https://doi.org/10.1371/journal.pone.0146021.

Roth, F., C. Wild, S. Carvalho, et al. 2019. "An In Situ Approach for Measuring Biogeochemical Fluxes in Structurally Complex Benthic Communities." *Methods in Ecology and Evolution* 10: 712–725. https://doi.org/10.1111/2041-210X.13151.

Rüegg, J., J. D. Brant, D. M. Larson, M. T. Trentman, and W. K. Dodds. 2015. "A Portable, Modular, Self-Contained Recirculating Chamber to Measure Benthic Processes under Controlled Water Velocity." *Freshwater Science* 34: 831–844. https://doi.org/10.1086/682328.

Schmitz, O. J., P. Raymond, J. Estes, et al. 2014. "Animating the Carbon Cycle." *Ecosystems* 17: 344–359. https://doi.org/10.1007/s10021-013-9715-7.

Schmitz, O. J., C. C. Wilmers, S. J. Leroux, et al. 2018. "Animals and the Zoogeochemistry of the Carbon Cycle." *Science* 362: eaar3213. https://doi.org/10.1126/science.aar3213.

Tank, J. L., J. L. Meyer, D. M. Sanzone, et al. 2000. "Analysis of Nitrogen Cycling in a Forest Stream during Autumn Using a ^{15}N-Tracer Addition." *Limnology and Oceanography* 45: 1013–1029. https://doi.org/10.4319/lo.2000.45.5.1013.

USEPA. 1982. Method 120.1: Conductance (Specific Conductance, μmhos at 25°C) by Conductivity Meter. Washigton, DC: US Environmental Protection Agency.

Vanni, M. J. 2002. "Nutrient Cycling by Animals in Freshwater Ecosystems." *Annual Review of Ecology and Systematics* 33: 341–370. https://doi.org/10.1146/annurev.ecolsys.33.010802.150519.

Vogel, S. 1996. Life in Moving Fluids: The Physical Biology of Flow. 2nd ed. New Jersey: Princeton University Press.

Whitaker, S. 1986. "Flow in Porous Media I: A Theoretical Derivation of Darcy's Law." *Transport in Porous Media* 1: 3–25. https://doi.org/10.1007/BF01036523.

Supporting Information

Additional Supporting Information may be found in the online version of this article.

Submitted 17 February 2025
Revised 10 April 2025
Accepted 07 May 2025